International Journal of Pharmacology

Int. J. Pharmacol. **2026**; 22(7): 52558
https://doi.org/10.31083/IJP52558

Research Article

Hydrogen Sulfide Alleviates Myocardial Ischemia/Reperfusion Injury Through Ferroptosis Inhibition via Activation of the Nrf2 Pathway

Xiaodong Jiang[1], Xuchen Han[2,*], Huiyan Sun[3,*]

[1]Department of Anatomy, College of Basic Medicine, Chifeng University Health Science Center, 024005 Chifeng, Inner Mongolia, China
[2]Department of Cardiology, The Affiliated Hospital of Chifeng University, 024005 Chifeng, Inner Mongolia, China
[3]Chifeng University Health Science Center, Chifeng University, 024000 Chifeng, Inner Mongolia, China
*Correspondence: Hanxuchen2004@163.com (Xuchen Han); shy1980_1981@163.com (Huiyan Sun)
Academic Editors: Mehmet Ozaslan and Giovanna Rigillo
Submitted: 25 February 2026 Revised: 8 May 2026 Accepted: 26 May 2026 Published: 20 November 2026

Abstract

Background: Myocardial ischemia/reperfusion injury (MIRI) remains a major challenge in the management of acute myocardial infarction. Ferroptosis, an iron-dependent form of regulated cell death, has been implicated in the pathogenesis of MIRI. Hydrogen sulfide (H_2S) exerts cardioprotective effects; however, whether H_2S alleviates MIRI by inhibiting ferroptosis through activation of the nuclear factor erythroid 2-related factor 2 (Nrf2) pathway remains unclear. **Methods:** An *in vivo* rat model of MIRI (30 min of ischemia followed by 4 h of reperfusion) and an *in vitro* H9C2 cardiomyocyte model of oxygen-glucose deprivation/reoxygenation (OGD/R) were used. Sodium hydrosulfide (NaHS) (an H_2S donor) was administered at 3 mg/kg intraperitoneally (i.p.) 4 hours after reperfusion in rats and 100 μM in cells. The ferroptosis inducer erastin was used to confirm the involvement of ferroptosis. Myocardial infarct size, inflammatory cytokines (TNF-α, IL-1β, IL-6), lactate dehydrogenase (LDH) and creatine kinase (CK) release, glutathione (GSH) levels, lipid peroxidation products (MDA, 4-HNE), iron accumulation, and protein expression of Nrf2, solute carrier family 7 member 11 (SLC7A11), and glutathione peroxidase 4 (GPX4) were assessed. **Results:** H_2S treatment significantly reduced myocardial infarct size, suppressed inflammatory cytokine levels, decreased LDH and CK release, restored GSH levels, reduced MDA and 4-HNE, and decreased iron accumulation *in vivo*. These effects were accompanied by upregulation of Nrf2, SLC7A11, and GPX4 protein expression. *In vitro*, H_2S improved cell viability, reduced reactive oxygen species (ROS) production and inflammatory cytokine levels, and inhibited ferroptotic changes, all of which were reversed by erastin. **Conclusions:** H_2S alleviates MIRI by inhibiting ferroptosis through activation of the Nrf2 signaling pathway. These findings provide new insight into the cardioprotective mechanisms of H_2S and suggest that targeting ferroptosis via Nrf2 may represent a potential therapeutic strategy for MIRI.

Keywords: myocardial infarction; reperfusion injury; hydrogen sulfide; ferroptosis; Nrf2

1. Introduction

Cardiovascular events are the leading cause of morbidity and mortality worldwide, with acute myocardial infarction (AMI) accounting for a significant proportion of deaths [1,2,3]. Reperfusion therapy remains the most effective treatment for AMI; however, this therapy can paradoxically aggravate myocardial damage, a phenomenon termed myocardial ischemia/reperfusion injury (MIRI), thereby impairing the benefits of restoring coronary blood flow [4].

Ferroptosis is a form of regulated cell death characterized by iron-dependent lipid peroxidation [5,6]. Accumulating evidence indicates that ferroptosis plays a pivotal role in the pathogenesis of MIRI and that targeted inhibition of ferroptosis can effectively reduce the severity of MIRI [7,8,9,10]. For example, the ferroptosis inhibitor ferrostatin-1 (Fer-1) and iron chelators have been shown to mitigate ischemia/reperfusion (I/R)-induced heart failure in animal models [8].

Hydrogen sulfide (H_2S) is an endogenous gasotransmitter with well-established cardioprotective effects against myocardial ischemia [5,11,12]. However, whether H_2S alleviates MIRI by inhibiting ferroptosis remains unclear. Therefore, this study tested the hypothesis that H_2S attenuates MIRI by suppressing ferroptosis through activation of the nuclear factor erythroid 2-related factor 2 (Nrf2) pathway, using both *in vivo* rat MIRI models and *in vitro* H9C2 cardiomyocyte oxygen-glucose deprivation/reoxygenation (OGD/R) models.

2. Materials and Methods

2.1 Materials

The CCK-8 kit was purchased from Wanleibio (WLA074, Shenyang, China). Sodium hydrosulfide (NaHS), an H_2S donor (intraperitoneal injection, 3 mg/kg; Cat# LS7485), and the fluorescent dye 2′,7′-dichlorodihydrofluorescein diacetate (D837204) were obtained from Macklin Inc. (China). Dulbecco's Modified Eagle Medium (DMEM) was purchased from Gibco Invitrogen Corporation. Antibodies against solute carrier family 7 member 11 (SLC7A11) (WLA0228), glutathione peroxidase 4 (GPX4) (WL05406), Nrf2 (WL02135), Histone H3 antibody (WL0984a), and β-actin (WL01372) were pur-

Copyright: © 2026 The Author(s). Published by IMR Press.
This is an open access article under the CC BY 4.0 license.

Publisher's Note: IMR Press stays neutral with regard to jurisdictional claims in published maps and institutional affiliations.

chased from Wanleibio (Shenyang, China). 12LOX antibody (sc-365194) was purchased from santa (USA). The 4-HNE antibody (MAB3249-SP) was obtained from NOVUS (Centennial, CO 80112, USA). C11-BODIPY581/591 (MX5211) was purchased from MKBio (Shanghai, China). The Iron Kit (BC5415) was from Solarbio Life Sciences (Beijing, China), and the GSH/GSSG kit (E-BC-K881-M) was obtained from Elabscience Biotechnology Co., Ltd. (Wuhan, China). The MDA kit (WLA048) and enzyme-linked immunosorbent assay (ELISA) kits for IL-6 (WLE04), IL-1β (WLE03), and TNF-α (WLE05) were purchased from Wanleibio (Shenyang, China). The 4-hydroxynonenal (4-HNE) ELISA kit (EU0187) was from Wuhan Fine. The ECL detection kit was obtained from Beyotime (Beijing, China), and the Complete Protease Inhibitor was purchased from Roche Diagnostics GmbH (Penzberg, Germany). All other chemicals used were commercially available and of high analytical grade.

2.2 Animal Model of MIRI

All animal procedures were performed in accordance with approved institutional guidelines. Male Sprague-Dawley (SD) rats (2 months old) were randomly assigned to experimental groups. Rats were anesthetized with 3% isoflurane in 99.5% O_2 and maintained under anesthesia with 2% isoflurane. MIRI was induced by ligating the left anterior descending coronary artery for 30 min, followed by 4 h of reperfusion (i.e., at the end of the 4-h reperfusion period), as previously described [13]. NaHS was administered via intraperitoneal injection at a dose of 3 mg/kg 4 h after reperfusion. Sham-operated rats underwent the same surgical procedure without coronary artery ligation. At 48 h after NaHS treatment, the rats were humanely euthanized in a CO_2 chamber, and cervical dislocation was performed to confirm death. Notably, 100% CO_2 was infused into the euthanasia chamber at a rate that replaced 10%–30% of the chamber volume per minute, ensuring complete filling of the chamber with CO_2. Subsequently, myocardial tissues were collected for further analysis.

2.3 TTC Staining

Hearts were removed and immediately perfused with phosphate-buffered saline (PBS), then frozen at –70 °C and sectioned transversely into 5 slices. These slices were stained with 1% 2,3,5-triphenyltetrazolium chloride (TTC) at 37 °C for 15 min. The white area of the heart, which was negatively stained by TTC, represented the infarcted tissue.

2.4 Myocardial Injury Marker Assay

Myocardial injury markers, including creatine kinase (CK) and lactate dehydrogenase (LDH), were measured as follows [13]: Blood was collected via abdominal aortic sampling and centrifuged using a low-temperature, high-speed centrifuge. The serum was then harvested and assayed in strict accordance with the manufacturers' instructions using commercial kits (CK kit, Nanjing Jiancheng Bioengineering Institute, China, Cat# H197-1-1; LDH kit, Nanjing Jiancheng Bioengineering Institute, China, Cat# A020-2-1).

2.5 Establishment of the OGD/R Model

The culture medium of H9C2 cells (Cat# iCell-r012, iCell Bioscience Inc., Shanghai, China) was replaced with glucose-free DMEM, and the cells were incubated at 37 °C under 5% CO_2 and 95% N_2 for 6 h. Then, the glucose-free medium was replaced with complete DMEM, and the cells were cultured under normoxic conditions at 37 °C and 5% CO_2 for 18 h to establish the OGD/R model.

2.6 Cell Culture and Treatment

H9C2 rat cardiomyocytes were cultured in DMEM supplemented with 10% fetal bovine serum (FBS) under conventional conditions at 37 °C and 5% CO_2. All cell lines were validated by STR profiling and tested negative for mycoplasma. Cells in the logarithmic growth phase were used for subsequent experiments. The H9C2 cells were adjusted to an optimal state and assigned to the following groups: cells routinely cultured under normal conditions (Sham); cells subjected to the OGD/R model without any pretreatment (OGD/R); cells treated with 100 μM NaHS for 30 min before establishment of the OGD/R model (OGD/R + NaHS); cells first treated with 5 μM of the ferroptosis inducer erastin for 24 h, then treated with 100 μM NaHS for 30 min prior to OGD/R induction (OGD/R + NaHS + erastin).

2.7 Cell Viability Assay

Cell viability was evaluated using CCK-8 kits (WLA074, Wanleibio, China) according to the manufacturer's protocol. Briefly, log-phase cells were seeded into 96-well plates at a density of 1×10^4 cells per well. Following 24 h of incubation, the cells were washed with PBS and incubated with 10 μL of CCK-8 reagent at 37 °C for 3 h. The absorbance was measured at 450 nm using a microplate reader.

2.8 Quantification of Cytokines and Detection of Tissue Iron

Heart tissue samples were accurately weighed, and 9 volumes (*i.e.*, 9 mL per 1 g of tissue) of homogenization medium (0.9% saline) were added to prepare a 10% homogenate. Inflammatory cytokine levels were analyzed using a sandwich ELISA. The levels of IL-1β (Wanleibio, Shenyang, China; 1:50 dilution; catalog no. WLE03), IL-6 (Wanleibio, Shenyang, China; 1:50 dilution; catalog no. WLE04), and TNF-α (Wanleibio, Shenyang, China; 1:50 dilution; catalog no. WLE05) were determined from the supernatant [14]. All procedures were performed strictly in accordance with the manufacturers' instructions. Tissue iron concentrations were also determined in accordance with the corresponding kit guidelines.

2.9 Glutathione (GSH) Measurement

The concentrations of total GSH and oxidized glutathione (GSSG) in both cells and tissues were determined using a T-GSH/GSSG Detection Assay kit, following the manufacturer's protocol.

2.10 Detection of Intracellular Reactive Oxygen Species (ROS) Generation

The intracellular ROS levels were measured using an intracellular ROS fluorescence assay kit (WLA131; Wanleibio, China) in accordance with the manufacturer's instructions. After collection, cells were resuspended in diluted DCFH-DA and incubated in a 37 °C cell culture incubator for 20 min, with gentle inversion every 3–5 min to ensure adequate probe–cell contact. After incubation, cells were washed three times with serum-free culture medium, centrifuged at 150 ×g for 5 min, washed once with PBS, and immediately analyzed by flow cytometry. Flow cytometric acquisition was performed on a NovoCyte flow cytometer (Agilent, USA). Intracellular ROS oxidize nonfluorescent DCFH to the strongly green-fluorescent product DCF, which has an excitation wavelength of 488 nm and a maximum emission peak at approximately 525 nm; the fluorescence intensity is proportional to the intracellular ROS level. For analysis, debris was excluded by gating the main cell population with an intermediate, continuous distribution on FSC-H versus SSC-H. The mean fluorescence intensity (MFI) of DCF in the gated single-cell population was used to quantify intracellular ROS levels.

2.11 BODIPY 581/591 C11 Assay

Detection of lipid ROS by C11-BODIPY 581/591 flow cytometry. Cells were collected, centrifuged at 150 ×g for 5 min, and the supernatant was carefully removed. Cells were washed once with PBS, centrifuged again at 150 ×g for 5 min, and resuspended in 5 µmol/L C11-BODIPY 581/591 (MKbio, Shanghai, China). After gentle mixing, cells were incubated in a 37 °C incubator for 30 min, washed three times with PBS, and resuspended in 500 µL PBS for immediate flow cytometric analysis. Flow cytometric acquisition was performed using conventional FITC (510 nm) emission filters to detect the oxidized (green) forms of the probe. For analysis, debris was excluded by gating the main cell population with an intermediate, continuous distribution on FSC-H versus SSC-H. The mean fluorescence intensity (MFI) in the FITC channel was quantified, and the FITC MFI was used as the measure of lipid ROS levels.

2.12 Detection of Malondialdehyde (MDA) and 4-Hydroxynonenal (4-HNE) Levels

The levels of MDA (WLA048; Wanleibio, China) and 4-HNE (EU0187; Wuhan Fine, China) were measured using the corresponding kits following the manufacturers' instructions.

2.13 Determination of Intracellular Iron Levels

Intracellular iron levels were measured using the iron assay kit (BC5415, Solarbio Life Sciences, China). The concentration of iron ions was measured at 520 nm using a microplate reader, and intracellular iron ion levels were normalized to cell number. Additionally, H9C2 cells were treated with 1 µM FerroOrange (Dojindo, Kumamoto, Japan) at 37 °C for 30 min, and the intracellular iron concentration was observed using a fluorescence microscope (Olympus, Tokyo, Japan).

2.14 Western Blot Analysis

Protein expression levels were analyzed by Western blotting. Myocardial tissue samples and H9C2 cells were homogenized in ice-cold RIPA buffer (Beyotime, China) and incubated on ice for 15 min. For subcellular fractionation, the homogenates were centrifuged at 3000 ×g and 4 °C for 10 min. The supernatant was collected as the cytosolic fraction. The nuclear pellet was washed twice with buffer A, resuspended in ice-cold RIPA buffer, incubated on ice for 30 min with intermittent vortexing, and centrifuged at 12,000 ×g and 4 °C for 15 min to obtain the nuclear fraction. Protein concentrations were determined using a BCA assay (Beyotime). Equal amounts of protein (30–50 µg) from each fraction or from whole lysates were separated by 10% sodium dodecyl sulfate–polyacrylamide gel electrophoresis (SDS–PAGE) and transferred to polyvinylidene fluoride (PVDF) membranes. After blocking with 5% bovine serum albumin, membranes were incubated overnight at 4 °C with primary antibodies (*e.g.*, Nrf2, SLC7A11, GPX4, β-actin, histone H3), followed by incubation with the corresponding secondary antibodies. Protein bands were detected using an ECL Plus chemiluminescence reagent kit (Pierce, USA) and quantified by densitometric analysis with ImageJ software (v1.4, NIH, USA). β-actin and histone H3 served as cytosolic and nuclear loading controls, respectively. All experiments were performed in triplicate.

2.15 Statistical Analysis

All data are presented as the mean ± standard error of the mean (S.E.M). Statistical analysis was performed using one-way analysis of variance (ANOVA) or Student's *t*-test with GraphPad Prism 6.0 software (GraphPad Software, Inc., San Diego, CA, USA). A p-value < 0.05 was considered statistically significant.

3. Results

3.1 H_2S Attenuates Myocardial Injury

To evaluate the cardioprotective effect of H_2S against MIRI, male SD rats were administered with NaHS (3 mg/kg) via intraperitoneal injection 4 hours after reperfusion. Histological and biochemical analyses were performed to assess myocardial injury. TTC showed extensive infarcted areas in MIRI rats, confirming severe necro-

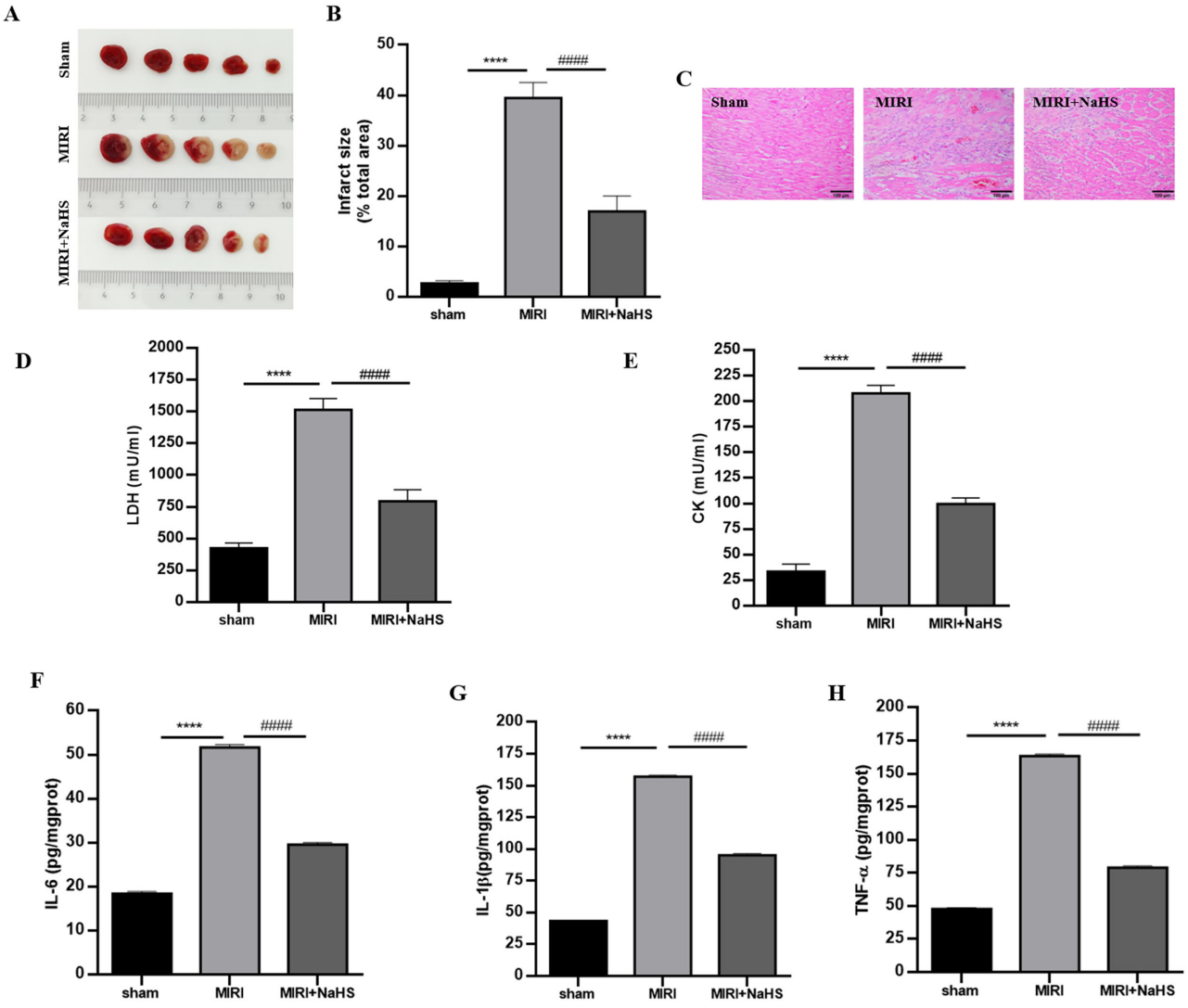

Fig. 1. The effects of H_2S on myocardial ischemia/reperfusion (I/R) injury in rat hearts. Male Sprague-Dawley (SD) rats were subjected to 30 min of ischemia followed by 4 h of reperfusion. NaHS (3 mg/kg), intraperitoneally [i.p.] was administered after 4 h of reperfusion (i.e., at the end of the 4-h reperfusion period). (A) Representative TTC-stained left ventricular sections of the infarct area (white). (B) Quantification of infarct size (% of total area). (C) Hematoxylin and eosin (H&E) staining (scale bar = 100 μm) of the pathological changes. (D) Serum LDH and (E) CK levels were measured using commercial kits. Myocardial concentrations of (F) IL-6, (G) IL-1β, and (H) TNF-α were determined by ELISA. Abbreviations: I/R, ischemia/reperfusion; NaHS, sodium hydrosulfide (H_2S donor); TTC, triphenyltetrazolium chloride; LDH, lactate dehydrogenase; CK,creatine kinase. Data are presented as the mean ± standard error of the mean (SEM) (n = 6/group). $^{****}p < 0.001$; $^{\#\#\#\#}p < 0.001$.

sis (Fig. 1A). NaHS treatment administered 4 h before surgery significantly reduced infarct size (Fig. 1B). Hematoxylin and eosin (H&E) staining revealed marked inflammatory cell infiltration and structural disorganization in MIRI hearts, both of which were alleviated by H_2S (Fig. 1C). Serological analysis demonstrated increased serum LDH and CK levels after I/R injury, whereas NaHS pretreatment markedly reduced both (Fig. 1D,E). Moreover, NaHS suppressed the I/R-induced inflammatory response, decreasing IL-6, IL-1β, and TNF-α levels (Fig. 1F–H).

3.2 H_2S Inhibits Ferroptosis in MIRI

To determine whether H_2S protects against MIRI by inhibiting ferroptosis, we measured myocardial levels of iron, glutathione (GSH), and oxidized glutathione (GSSG). IRI increased GSSG and reduced GSH in myocardial tissue. In contrast, NaHS treatment increased GSH (Fig. 2A) and increased GSH/GSSG (Fig. 2B). Measurement of the lipid peroxidation products 4-HNE and MDA showed that IRI promoted lipid peroxidation, an effect that was reversed by NaHS (Fig. 2C,D). IRI also increased myocardial iron content, which was reduced by NaHS (Fig. 2E). Consis-

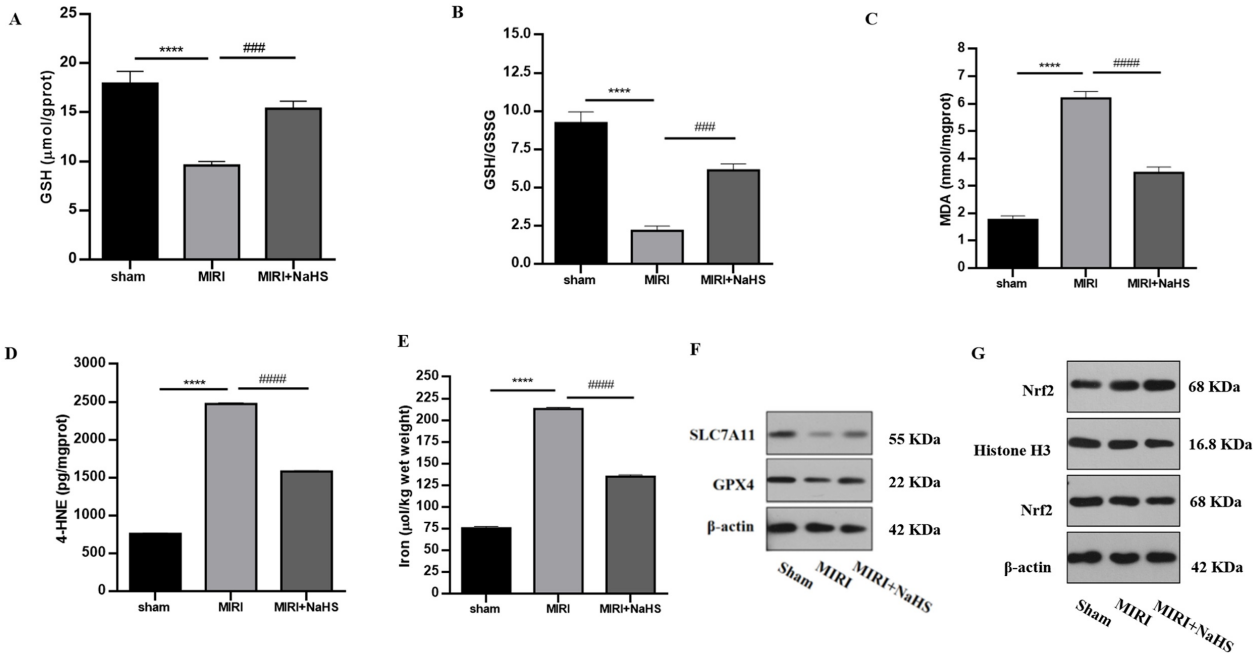

Fig. 2. H_2S inhibits ferroptosis in myocardial ischemia/reperfusion (I/R) injury in rats. Male SD rats underwent 30 min of ischemia followed by 4 h of reperfusion. NaHS (3 mg/kg, i.p.) was administered 4 h after reperfusion (as described in Fig. 1). (A) Reduced glutathione (GSH) levels. (B) Ratio of GSH to oxidized glutathione (GSSG). (C) Malondialdehyde (MDA) content. (D) 4-Hydroxynonenal (4-HNE) levels. (E) Iron content in myocardial tissue. (F) Western blot analysis of SLC7A11 and GPX4 protein expression in myocardial lysates; β-actin was used as the loading control. (G) Nuclear and cytosolic Nrf2 protein levels were detected by Western blot. Abbreviations: GSH, glutathione; GSSG, oxidized glutathione; MDA, malondialdehyde; 4-HNE, 4-hydroxynonenal; SLC7A11, solute carrier family 7 member 11; GPX4, glutathione peroxidase 4; Nrf2, nuclear factor erythroid 2-related factor 2. Statistical annotations: Data are presented as mean ± SEM (n = 6 per group). $^{****}p < 0.001$; $^{###}p < 0.005$; $^{####}p < 0.001$.

tently, Western blot analysis revealed that IRI suppressed Nrf2 activation and reduced SLC7A11 and GPX4 protein levels, whereas NaHS restored the expression of these proteins (Fig. 2F,G). Collectively, these results indicate that NaHS significantly inhibits ferroptosis in MIRI rats.

3.3 Erastin Reverses Hydrogen Sulfide-Mediated Inhibition of Cell Injury in OGD/R-Induced H9C2 Cells

Next, we examined whether H_2S mitigates OGD-R-induced cardiomyocyte injury at the cellular level by inhibiting ferroptosis. Indeed, OGD/R decreased H9C2 cell viability (Fig. 3A), increased ROS production (Fig. 3B), and elevated inflammatory factor levels (Fig. 3C–E), whereas NaHS reversed these changes. However, erastin, which is a ferroptosis inducer, counteracted the inhibitory effect of NaHS on H9C2 cell injury. Collectively, these findings indicate that erastin reverses the protective effect of NaHS on cardiomyocyte injury, suggesting that NaHS protects against OGD/R-induced cardiomyocyte damage by inhibiting ferroptosis.

3.4 Erastin Reverses Hydrogen Sulfide-Mediated Inhibition of Ferroptosis in OGD-R-Induced H9C2 Cells

To further confirm that H_2S alleviates OGD/R-induced H9C2 cell injury by suppressing ferroptosis, we applied erastin as a ferroptosis inducer. Erastin reversed the H_2S-mediated inhibition of ferroptosis, as evidenced by increased lipid ROS (Fig. 4A), MDA (Fig. 4B), and 4-HNE (Fig. 4C); decreased GSH levels (Fig. 4D) and GSH/GSSG ratio (Fig. 4E); and increased iron content (Fig. 4F,G). Additionally, erastin reversed the NaHS-induced upregulation of SLC7A11 and GPX4 (Fig. 4H), as well as Nrf2 (Fig. 4I). Collectively, these results indicate that H_2S attenuates OGD/R-induced injury in H9C2 cells through the suppression of ferroptosis.

4. Discussion

This study demonstrates that H_2S attenuates MIRI by inhibiting ferroptosis through activation of the Nrf2 pathway. Both *in vivo* and *in vitro* experiments consistently showed that H_2S significantly alleviates myocardial damage, reduces oxidative stress and inflammatory responses, and counteracts key ferroptotic events, including iron accumulation, lipid peroxidation, and depletion of antioxidant defenses.

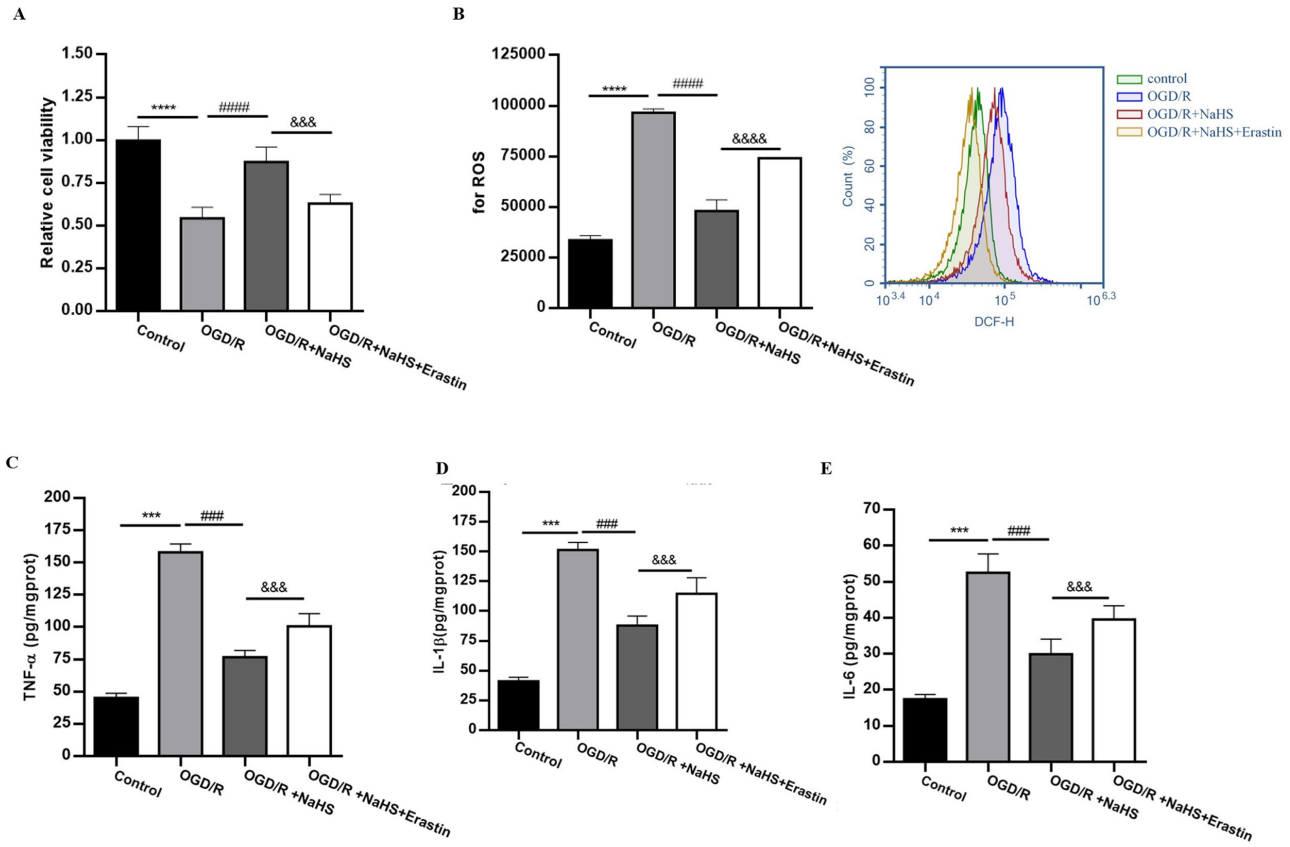

Fig. 3. Erastin reverses H_2S-mediated inhibition of cell injury in oxygen–glucose deprivation/reoxygenation (OGD/R)-induced H9C2 cells. Rat cardiomyocytes (H9C2) were pretreated with erastin (5 μM) for 24 h, followed by NaHS (100 μM) for 30 min, then subjected to oxygen-glucose deprivation (OGD) for 6 h (glucose-free medium under 95% N_2/5% CO_2) and reoxygenation for 18 h (normal medium under 95% air/5% CO_2). (A) Cell viability (CCK-8 assay). (B) Intracellular reactive oxygen species (ROS) levels (DCFH-DA fluorescence). (C–E) TNF-α, IL-1β, and IL-6 in cell lysates (ELISA). Data are presented as the mean ± SEM (n = 3 independent experiments). $^{\#\#\#}p < 0.005$; $^{\#\#\#\#}p < 0.001$; $^{***}p < 0.005$; $^{****}p < 0.001$; $^{\&\&\&}p < 0.005$; $^{\&\&\&\&}p < 0.001$.

Our results indicate that H_2S treatment markedly reduced infarct size, improved cardiac function, and decreased levels of myocardial injury markers (LDH and CK) in MIRI rats. These findings are consistent with previous studies that highlight the cardioprotective effects of H_2S across various models of cardiac injury [15,16,17,18]. Importantly, this study provides novel evidence that these beneficial effects are mediated, at least in part, through the suppression of ferroptosis. Specifically, H_2S restored glutathione homeostasis, reduced levels of lipid peroxidation products (MDA and 4-HNE), and decreased intracellular iron accumulation. Moreover, H_2S upregulated the expression of key anti-ferroptotic proteins, including SLC7A11, GPX4, and Nrf2. The reversal of H_2S-mediated protection by the ferroptosis inducer erastin further supports the essential role of ferroptosis inhibition in the mechanism of H_2S action. In H9C2 cells subjected to OGD/R, erastin abolished the beneficial effects of H_2S on cell viability, ROS production, inflammatory cytokine release, and ferroptosis-related biochemical changes. These findings confirm that H_2S exerts cytoprotective effects specifically by modulating ferroptotic pathways.

Activation of the Nrf2 pathway is central to H_2S-mediated inhibition of ferroptosis. Nrf2 regulates antioxidant response elements, controlling genes involved in iron metabolism, redox balance, and glutathione synthesis, including *SLC7A11* and *GPX4* [19,20,21,22,23,24]. Our data confirm that H_2S enhances Nrf2 activation and upregulates downstream targets associated with Nrf2, consistent with the known role of Nrf2 in mitigating ferroptosis. Mechanistically, H_2S activates Nrf2 via multiple pathways: H_2S S-sulfhydrates (persulfidates) Keap1 at critical cysteine residues (*e.g.*, Cys151, Cys273, Cys288), disrupting Keap1–Nrf2 binding and preventing Nrf2 ubiquitination and degradation [25,26]. This stabilizes Nrf2, promotes the nuclear translocation of Nrf2, and drives the transcription of associated antioxidant and anti-ferroptotic genes. Additionally, H_2S activates upstream kinases such as AMPK, PI3K/Akt, and PKC, which phosphorylate Nrf2 and further enhance the nuclear accumulation of Nrf2 [27,28,29]. To-

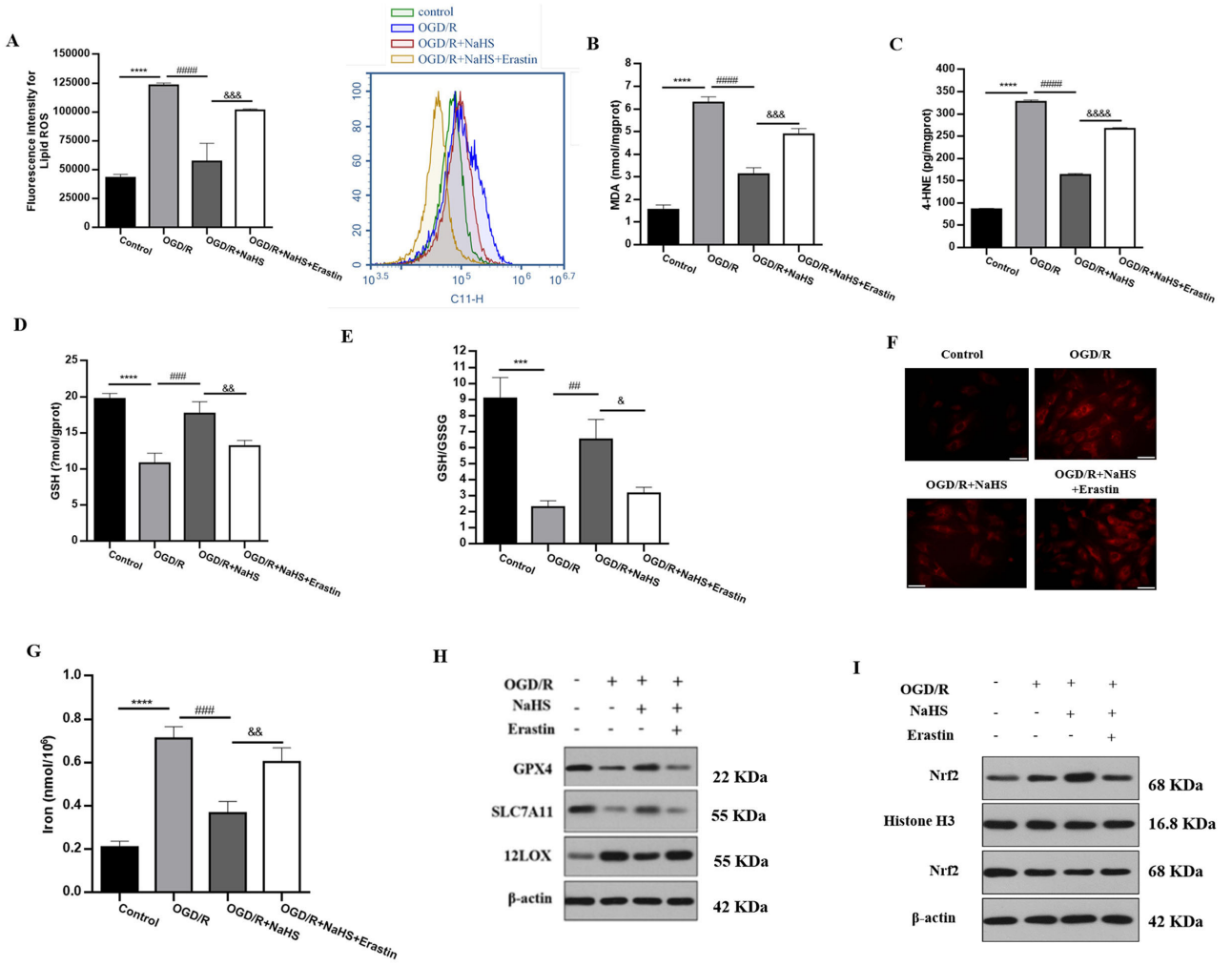

Fig. 4. Erastin reverses H_2S-mediated inhibition of ferroptosis in OGD/R-exposed H9C2 cells. Experimental procedures were performed as described in Fig. 3. The following parameters were assessed: (A) lipid ROS levels using C11-BODIPY581/591 fluorescence; (B) MDA content; (C) 4-HNE levels; (D) GSH levels; (E) GSH/GSSG ratio; (F) representative FerroOrange staining images for intracellular Fe^{2+} (scale bar = 50 μm); (G) quantitative iron content; (H) Western blot analysis of 12 LOX, SLC7A11 and GPX4 (β-actin as loading control); (I) nuclear and cytosolic Nrf2 protein expression. Abbreviations: lipid ROS, lipid reactive oxygen species; Fe^{2+}, ferrous iron. Data are presented as the mean ± SEM (n = 3 independent experiments). Statistical annotations are as indicated in the figure. $^{\#\#}p < 0.01$; $^{\#\#\#}p < 0.005$; $^{\#\#\#\#}p < 0.001$; $^{***}p < 0.005$; $^{****}p < 0.001$; $^{\&}p < 0.05$; $^{\&\&}p < 0.01$; $^{\&\&\&}p < 0.005$; $^{\&\&\&\&}p < 0.001$. MDA, malondialdehyde; 4-HNE, 4-hydroxynonenal; GSH, glutathione.

gether, these mechanisms establish H_2S as a potent Nrf2 activator, linking its cardioprotective effects to ferroptosis inhibition in MIRI.

These findings both expand our understanding of the pharmacological mechanisms of H_2S and highlight ferroptosis as a promising therapeutic target for MIRI. Although this study provides compelling evidence, further research is required to elucidate the detailed signaling cascades linking H_2S to Nrf2 activation and to explore the potential clinical application of H_2S-based therapies in ischemic heart disease.

5. Limitation

While this study provides strong evidence that hydrogen sulfide alleviates MIRI by inhibiting ferroptosis via Nrf2 activation, several limitations warrant acknowledgment. First, the *in vivo* experiments were conducted exclusively in male SD rats, leaving potential sex-dependent effects of H2S on ferroptosis and cardioprotection unexplored. Second, although NaHS is a well-established H2S donor, the rapid release kinetics of NaHS may not fully recapitulate sustained physiological levels of endogenous H2S; therefore, future studies employing slow-release or targeted H2S donors would be valuable. Third, the mechanistic role of Nrf2 was inferred primarily from changes

in protein expression and the use of a ferroptosis inducer (erastin), without genetic loss- or gain-of-function approaches (e.g., Nrf2 siRNA or knockout animals) to definitively establish causality. Fourth, the *in vitro* work relied on the H9C2 cardiomyocyte cell line, which is of embryonic rat origin and may not fully mirror the responses of adult primary cardiomyocytes. Fifth, the study focused on acute (4 h reperfusion) and subacute (48 h) endpoints; long-term effects on cardiac remodeling, function, and survival were not assessed. Finally, the potential contributions of other cell death pathways (e.g., apoptosis, necroptosis) and the crosstalk between these pathways and ferroptosis were not systematically examined. Addressing these limitations in future investigations will further solidify the therapeutic potential of targeting the H2S–Nrf2–ferroptosis axis in MIRI.

6. Conclusion

In conclusion, this study reveals that H_2S protects against MIRI by inhibiting ferroptosis via activation of the Nrf2 pathway, offering new insights into the molecular basis of H_2S-induced cardioprotection and supporting the development of novel therapeutic strategies targeting ferroptosis in cardiovascular diseases.

Availability of Data and Materials

The datasets generated and analyzed during the current study are not publicly available because further research is needed, but they are available from the corresponding authors upon reasonable request.

Author Contributions

XJ, XH and HS conceived of and designed the study. XJ and HS performed methodology, data curation, formal analysis, and visualization. XH provided administrative support. XJ and HS wrote the manuscript. All authors analysed and interpreted the data. All authors read and approved the final manuscript. All authors contributed to editorial changes in the manuscript. All authors have participated sufficiently in the work and agreed to be accountable for all aspects of the work.

Ethics Approval and Consent to Participate

This study was carried out in accordance with theARRIVE guidelines and principles of the Basel Declaration and recommendations of Chifeng University for laboratory animals. The animal study was reviewed and approved by Medical ethics committee of Chifeng University (2024-1-NM001).

Acknowledgment

Not applicable.

Funding

This work was supported in part by the Natural Science Foundation of Inner Mongolia Autonomous Region (2023LHMS08050).

Conflicts of Interest

The authors declare no conflicts of interest.

Supplementary Material

Supplementary material associated with this article can be found, in the online version, at https://doi.org/10.31083/IJP52558.

References

[1] Zalewski J, Nowak K, Furczynska P, Zalewska M. Complicating Acute Myocardial Infarction. Current Status and Unresolved Targets for Subsequent Research. Journal of Clinical Medicine. 2021; 10: 5904. https://doi.org/10.3390/jcm10245904

[2] Villa E, Saso L, Chichiarelli S, Rojas-Solé C, Pinilla-González V, Prieto JC, et al. Antioxidant Cardioprotection in Acute Myocardial Infarction: From Mechanisms to Therapeutic Strategies. Frontiers in Bioscience (Landmark Edition). 2025; 30: 27678. https://doi.org/10.31083/FBL27678

[3] Chang T, Jin Y, Fan C, Wang H, Jin L, Shi Y, et al. N-acetylglucosaminyltransferase V attenuates myocardial infarction by mediating the insulin-like growth factor 1 receptor signaling pathway. Journal of Translational Internal Medicine. 2025; 13: 281–294. https://doi.org/10.1515/jtim-2025-0021

[4] He C, Yang H, Xu L, Zhang H, Hu H. Fto-Mediated m6A Demethylation of Anxa1 Attenuates Cardiac Ischemia-Reperfusion Injury With Suppression of Nlrp3 Inflammasome Signals. Frontiers in Bioscience (Landmark Edition). 2025; 30: 42765. https://doi.org/10.31083/FBL42765

[5] Fang X, Wang H, Han D, Xie E, Yang X, Wei J, et al. Ferroptosis as a target for protection against cardiomyopathy. Proceedings of the National Academy of Sciences of the United States of America. 2019; 116: 2672–2680. https://doi.org/10.1073/pnas.1821022116

[6] Wang Y, Wang W, Zhang Y, Fleishman JS, Wang H. Targeting ferroptosis offers therapy choice in sepsis-associated acute lung injury. European Journal of Medicinal Chemistry. 2025; 283: 117152. https://doi.org/10.1016/j.ejmech.2024.117152

[7] Dixon SJ, Lemberg KM, Lamprecht MR, Skouta R, Zaitsev EM, Gleason CE, et al. Ferroptosis: an iron-dependent form of nonapoptotic cell death. Cell. 2012; 149: 1060–1072. https://doi.org/10.1016/j.cell.2012.03.042

[8] Yu Y, Yan Y, Niu F, Wang Y, Chen X, Su G, et al. Ferroptosis: a cell death connecting oxidative stress, inflammation and cardiovascular diseases. Cell Death Discovery. 2021, 7: 193. https://doi.org/10.1038/s41420-021-00579-w

[9] Zheng K, Dong Y, Yang R, Liang Y, Wu H, He Z. Regulation of ferroptosis by bioactive phytochemicals: Implications for medical nutritional therapy. Pharmacological Research. 2021; 168: 105580. https://doi.org/10.1016/j.phrs.2021.105580

[10] Liu S, Yang X, Zheng S, Chen C, Qi L, Xu X, et al. Research progress on the use of traditional Chinese medicine to treat diseases by regulating ferroptosis. Genes & Diseases. 2024; 12: 101451. https://doi.org/10.1016/j.gendis.2024.101451

[11] Zhao WK, Zhou Y, Xu TT, Wu Q. Ferroptosis: Opportunities and Challenges in Myocardial Ischemia-Reperfusion Injury. Oxidative Medicine and Cellular Longevity. 2021; 9929687. https://doi.org/10.1155/2021/9929687

[12] Sparvero LJ, Tian H, Amoscato AA, Sun WY, Anthonymuthu TS, Tyurina YY, et al. Direct Mapping of Phospholipid Ferroptotic Death Signals in Cells and Tissues by Gas Cluster Ion Beam Secondary Ion Mass Spectrometry (GCIB-SIMS). Angewandte Chemie (International ed. in English). 2021; 60: 11784–11788. https://doi.org/10.1002/anie.202102001

[13] Su Z, Li P, Ding W, Gao Y. Urolithin A improves myocardial ischemia-reperfusion injury by attenuating oxidative stress and ferroptosis through Nrf2 pathway. International Immunopharmacology. 2024; 143: 113394. https://doi.org/10.1016/j.intimp.2024.113394

[14] Han X, Yang Y, Zhang M, Li L, Xue Y, Jia Q, et al. Liquiritin protects against cardiac fibrosis after myocardial infarction by inhibiting CCL5 expression and the NF-κB signaling pathway. Drug Design, Development and Therapy. 2022; 16: 4111–4125. https://doi.org/10.2147/DDDT.S386805

[15] Zhan Y, Zhao X, Liu R, Bi S, Ge Y, Wang Y, et al. Alleviation of myocardial infarction by hydrogen sulfide-releasing nanoparticles: mechanisms and therapeutic effects. Journal of Materials Chemistry. B. 2025; 13: 8358–8367. https://doi.org/10.1039/d5tb00672d

[16] Zhang Q, Wang L, Yin Y, Shen J, Xie J, Yuan J. Hydrogen sulfide releasing hydrogel for alleviating cardiac inflammation and protecting against myocardial ischemia-reperfusion injury. Journal of Materials Chemistry. B. 2022; 10: 5344–5351. https://doi.org/10.1039/d2tb00971d

[17] Ansari M, Prem PN, Kurian GA. Hydrogen sulfide postconditioning rendered cardioprotection against myocardial ischemia-reperfusion injury is compromised in rats with diabetic cardiomyopathy. Microvascular Research. 2022; 141: 104322. https://doi.org/10.1016/j.mvr.2022.104322

[18] Zhang P, Yu Y, Wang P, Shen H, Ling X, Xue X, et al. Role of Hydrogen Sulfide in Myocardial Ischemia-Reperfusion Injury. Journal of Cardiovascular Pharmacology. 2021; 77: 130–141. https://doi.org/10.1097/FJC.0000000000000943

[19] Dodson M, Castro-Portuguez R, Zhang DD. NRF2 plays a critical role in mitigating lipid peroxidation and ferroptosis. Redox Biology. 2019; 23: 101107. https://doi.org/10.1016/j.redox.2019.101107

[20] Kajarabille N, Latunde-Dada GO. Programmed Cell-Death by Ferroptosis: Antioxidants as Mitigators. International Journal of Molecular Sciences. 2019; 20: 4968. https://doi.org/10.3390/ijms20194968

[21] Kerins MJ, Ooi A. The Roles of NRF2 in Modulating Cellular Iron Homeostasis. Antioxidants & Redox Signaling. 2018; 29: 1756–1773. https://doi.org/10.1089/ars.2017.7176

[22] Lane DJR, Metselaar B, Greenough M, Bush AI, Ayton SJ. Ferroptosis and NRF2: an emerging battlefield in the neurodegeneration of Alzheimer's disease. Essays in Biochemistry. 2021; 65: 925–940. https://doi.org/10.1042/EBC20210017

[23] Qu Z, Sun J, Zhang W, Yu J, Zhuang C. Transcription factor NRF2 as a promising therapeutic target for Alzheimer's disease. Free Radical Biology & Medicine. 2020; 159: 87–102. https://doi.org/10.1016/j.freeradbiomed.2020.06.028

[24] Tang D, Kang R. NFE2L2 and ferroptosis resistance in cancer therapy. Cancer Drug Resistance (Alhambra, Calif.). 2024; 7: 41. https://doi.org/10.20517/cdr.2024.123

[25] Yang G, Zhao K, Ju Y, Mani S, Cao Q, Puukila S, et al. Hydrogen sulfide protects against cellular senescence via S-sulfhydration of Keap1 and activation of Nrf2. Antioxidants & Redox Signaling. 2013; 18: 1906–1919. https://doi.org/10.1089/ars.2012.4645

[26] Xie L, Gu Y, Wen M, Zhao S, Wang W, Ma Y, et al. Hydrogen Sulfide Induces Keap1 S-sulfhydration and Suppresses Diabetes-Accelerated Atherosclerosis via Nrf2 Activation. Diabetes. 2016; 65: 3171–3184. https://doi.org/10.2337/db16-0020

[27] Calvert JW, Jha S, Gundewar S, Elrod JW, Ramachandran A, Pattillo CB, et al. Hydrogen sulfide mediates cardioprotection through Nrf2 signaling. Circulation Research. 2009; 105: 365–374. https://doi.org/10.1161/CIRCRESAHA.109.199919

[28] Peake BF, Nicholson CK, Lambert JP, Hood RL, Amin H, Amin S, et al. Hydrogen sulfide preconditions the db/db diabetic mouse heart against ischemia-reperfusion injury by activating Nrf2 signaling in an Erk-dependent manner. American Journal of Physiology. Heart and Circulatory Physiology. 2013; 304: H1215–H1224. https://doi.org/10.1152/ajpheart.00796.2012

[29] Wang R. Physiological implications of hydrogen sulfide: a whiff exploration that blossomed. Physiological Reviews. 2012; 92: 791–896. https://doi.org/10.1152/physrev.00017.2011